Atomic-Oxygen Durability of Impact-Damaged Solar Reflectors

Daniel A. Gulino*
NASA Lewis Research Center, Cleveland, Ohio

Silver mirror samples with protective coatings were subjected to a stream of 27-μm alumina particles to induce pinhole defects. The protective coating consisted of a layer of aluminum oxide over silver, followed by a layer of silicon dioxide over the alumina. Samples were prepared on both graphite-epoxy composite and fused quartz substrates. After exposure to the hard particle stream, the samples were exposed to an oxygen plasma environment in a laboratory plasma asher. The effects of both the hard particles and the oxygen plasma were documented by reflectance measurements and scanning electron microscopy. Results indicated that oxidative damage to the silver reflecting layer continues beyond that of the erosively exposed silver. Oxidative undercutting of the silver layer and graphite-epoxy substrate continues in undamaged areas through adjacent, particle-damaged defect sites. This may have implications for the use of such mirrors in a Space Station solar dynamic power system.

Introduction

ELECTRICAL power on the Space Station is currently envisioned to be generated by a combination of both photovoltaic and solar dynamic power systems. Solar dynamic systems generate electricity by reflecting and focusing the sun's energy onto the receiver of a heat engine. An important consideration in the use of a solar dynamic system in space is the survivabiity of the reflecting surface in the low Earth orbit (LEO) environment through which the Space Station will fly.

The major constituent of the LEO environment is neutral atomic oxygen.[1] This species is highly corrosive and is known to attack a number of materials.[2-4] If silver is used in the mirror as the reflecting medium, a transparent, protective coating must be applied to the surface to prevent oxidation of the silver by atomic oxygen. Other hazards presented by the LEO enviroment include micrometeoroids and orbiting space debris. If such particles should strike the surface of the mirror and pierce the protective coating, oxidative damage to both the underlying silver layer and the substrate is possible. It was the intent of the work to be described here to investigate the effect of particle impact damage on the continued atomic oxygen survivability of silver reflectors with transparent protective overcoats.

Apparatus and Procedure

Mirror samples were prepared by argon-ion beam sputtering from a silver target onto graphite-epoxy composite and fused quartz substrates in an apparatus described elsewhere.[5] The graphite-epoxy (Union Carbide T-300 fibers in a Fiberite 934 epoxy matrix) had been first polished to a smooth finish with diamond paste. The silver layer was approximately 2000 Å in thickness. The protective coating consisted of a layer of Al_2O_3 (approximately 700 Å) over the silver and then a layer of SiO_2 (approximately 2200 Å) over the Al_2O_3. This particular coating combination was chosen because it it typical of the protective coating systems under consideration for use on solar dynamic concentrator mirrors.

The atomic oxygen environment was simulated by use of a Structure Probe, Inc., Plasma Prep II laboratory plasma asher facility operated with air. This device creates the plasma by exciting a carrier gas (in this case, ambient air) with 100 W of continuous wave rf power at 13.56 MHz. Other work[6] has shown that any contribution by other constituents of air (mainly nitrogen) to the degradation observed would be negligible. The operating pressure is about 50 μ. Although it is difficult to form a direct correlation between exposure time in the asher and lifetime in LEO, use of the asher facility does allow gross determination of the likelihood of survivability of a particular material in LEO.

Impact damage and pinhole defects were imparted to the sample surfaces with a high-speed abrasive particle unit using 27-μm diam alumina particles. This unit accelerates the particles to a velocity of about 340 m/s (about 1100 ft/s) at a flux of about 6×10^{12} $cm^{-2}s^{-1}$.

Samples prepared on graphite-epoxy substrates were characterized by both reflectance measurements and scanning electron microscopy (SEM). Integrated solar reflectances were obtained by measuring the reflectance vs wavelength over the range 200-2500 nm and then convoluting this spectrum into the air-mass-zero-solar spectrum[7] over the same wavelength range.[8] In doing so, only about 3% of the solar constant is neglected. Such measurements were made for each graphite-epoxy sample as a function of length of time of exposure to both the particle flux and the oxygen plasma. Both total and specular reflectances were obtained, the latter of which were measured at an 8 deg angle of incidence, with an acceptance aperture solid angle of 0.096 sr. Samples prepared on fused quartz substrates were characterized only by SEM.

For the graphite-epoxy substrate samples, the procedure was to erode each sample for a different length of time, thereby causing the specular reflectance to fall by a different amount for each sample before exposure to the oxygen plasma. Samples were exposed to the particle flux for times ranging in length from 0 to 96 s. This caused by specular reflectance to fall from 0% to about 50% of the initial, noneroded reflectance. Additional reflectance measurements were then obtained on each sample after subsequent oxygen plasma exposure. For the fused quartz substrate samples, each was exposed to the particle flux for the same length of time (16 s) and then exposed to the oxygen plasma.

Presented as Paper 87-0104 at the AIAA 25th Aerospace Sciences Meeting, Reno, NV, Jan. 12-15, 1987; received Nov. 21, 1986; revision received March 25, 1987.

*Research Scientist, Power Technology Division. Member AIAA.

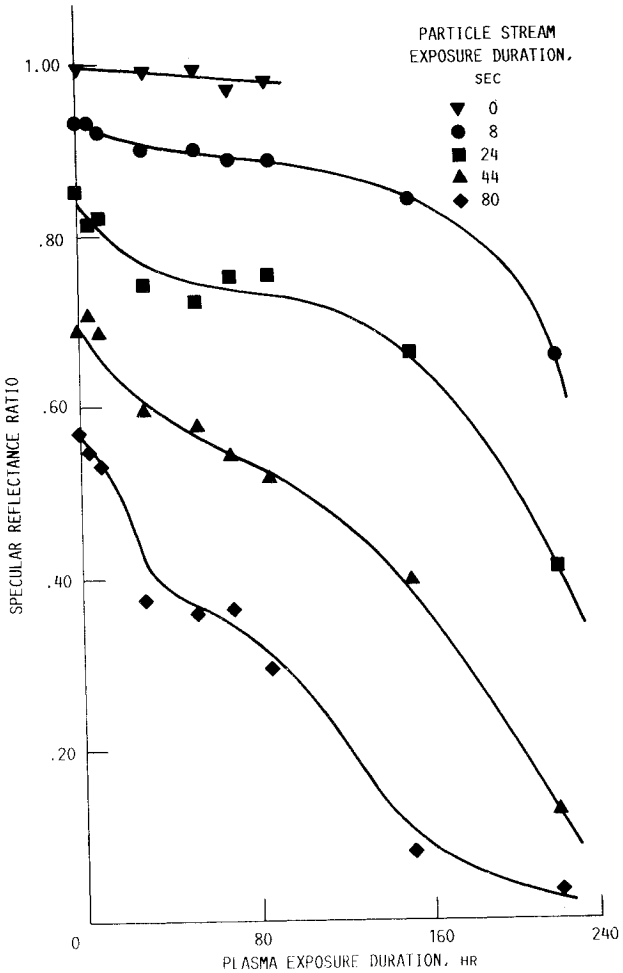

Fig. 1. Specular reflectance ratios vs plasma exposure time for several graphite-epoxy substrate samples for various lengths of time of exposure to the erosive particle stream. The ratio is calculated by dividing the reflectance at a given time by the reflectance measured prior to particle exposure.

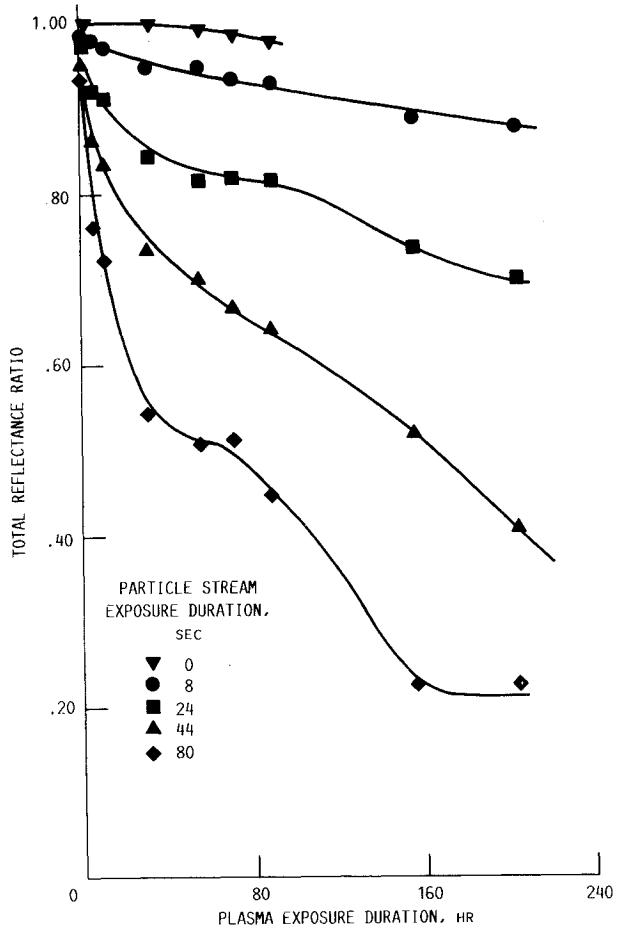

Fig. 2. Total reflectance ratio vs plasma exposure time for several graphite-epoxy substrate samples for various lengths of time of exposure to the erosive particle stream. The method of calculation is identical to that of Fig. 1.

Results

In Figs. 1 and 2 are plotted, respectively, the specular and total reflectance ratios of several of the graphite-epoxy substrate samples as a function of oxygen plasma exposure duration. The reflectance ratios were obtained by dividing the reflectance at a given time by the initial, noneroded, nonashed reflectance. The data points at zero hours thus indicate the effect on the reflectance of only the erosive particle stream as a function of duration of exposure to the particle stream. Scanning electron micrographs (to be discussed later) showed no evidence that any of the alumina particles adhered to the reflector surfaces on impact, at least as undamaged spheres. Particle fragments may have adhered to the surface, had any of the particles broken apart on impact. However, there was no visual evidence of any buildup of material (alumina) on these surfaces strictly as a function of particle exposure time.

In Figs. 1 and 2, three rather broadly defined regions can be observed. During the first roughly 30-h exposure, the reflectances fell rather markedly from their initial values, with the degree of fall directly proportional to the length of exposure time to the particle flux. For the next 60 h, the reflectances remained roughly constant. After this, they began to decrease once again, and with a rate of decrease that increased with time. These effects were somewhat more pronounced on the specular reflectance plots.

Scanning electron micrographs were obtained after a variety of different treatments and exposure times. Figure 3 is a micrograph of a noneroded, nonashed sample on a graphite-epoxy substrate. (The white, irregularly shaped object in the lower left is a dust particle that aided in focusing.) The only feature visible is the ridged structure of the graphite-epoxy substrate. Figure 4 is a micrograph of a sample similar to that in Fig. 3, except that this sample had been exposed to the particle stream. A number of defect sites are evident.

Figures 5–9 show the effect of exposure of the particle-eroded, graphite-epoxy substrate samples to the plasma for different lengths of time. Figure 5 is a micrograph of a sample that had been exposed in the asher for 50 h. While the region photographed is different from that of Fig. 4, the appearance of the regions is the same; a variety of differently sized and shaped defect sites. Figure 6 is a micrograph of a sample exposed in the asher for 90 h. The heart-shaped darkened "rim" surrounding the defect site at the lower left of this photo is a result of oxidation of the silver and/or the substrate surrounding that defect site. The width of the rim is very roughly the diameter of the pinhole defect. Figure 7 is an enlarged view of another defect site on the same sample as Fig. 6. Oxidative undercutting (the darkened rim) is clearly evident. Figure 8 is a micrograph of a sample exposed in the asher for 240 h.. In this figure, it is evident that oxidative undercutting has occurred to a large degree. The widths of the darkened rims are now nearly 10 times the diameter of the defect site.

These photos clearly show that although oxidative undercutting is a process that does not begin immediately, once it does start, its rate accelerates with increasing asher exposure time. This finding explains the shape of the reflectance vs exposure time curves shown in Figs. 1 and 2, particularly the

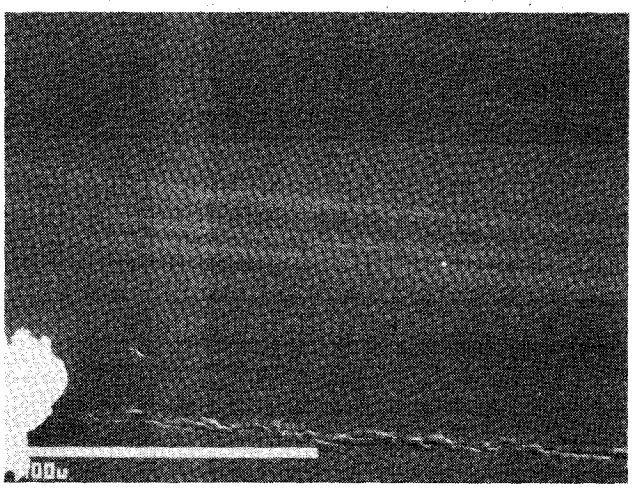

Fig. 3. Micrograph taken at 500× showing a noneroded, nonashed graphite-epoxy substrate sample. Only the ridged structure of the substrate is visible.

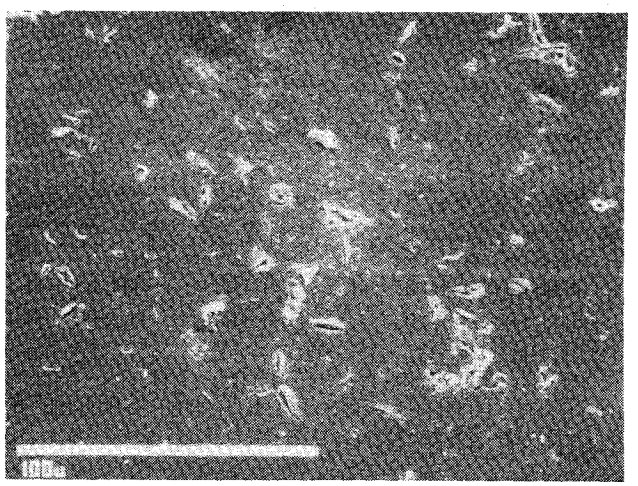

Fig. 4. Micrograph taken at 500× showing the effect of the erosive particle stream only (no plasma exposure) on a graphite-epoxy substrate sample. A number of defect sites are evident.

Fig. 5. Micrograph taken at 1000× showing a particle eroded surface after 50 h of exposure to the oxygen plasma. The appearance is similar to that of Fig. 4. No evidence of undercutting is visible.

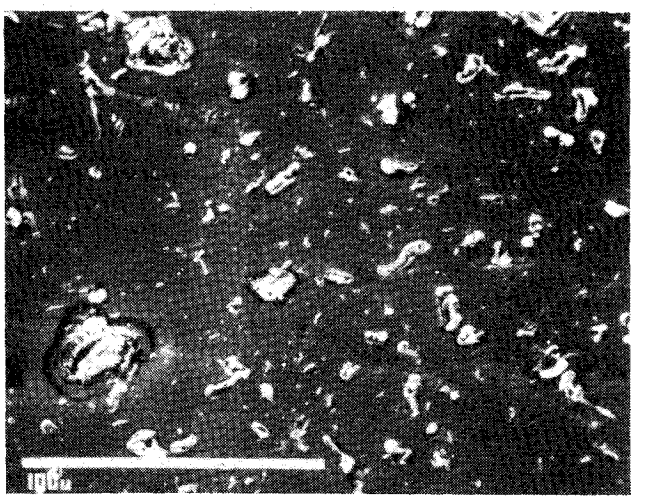

Fig. 6. Micrograph taken at 500× showing a particle eroded surface after 90 h of exposure to the oxygen plasma. The darkened "rim" surrounding the heart-shaped defect in the lower left is oxidation of the silver layer and/or the substrate beneath the protective coating.

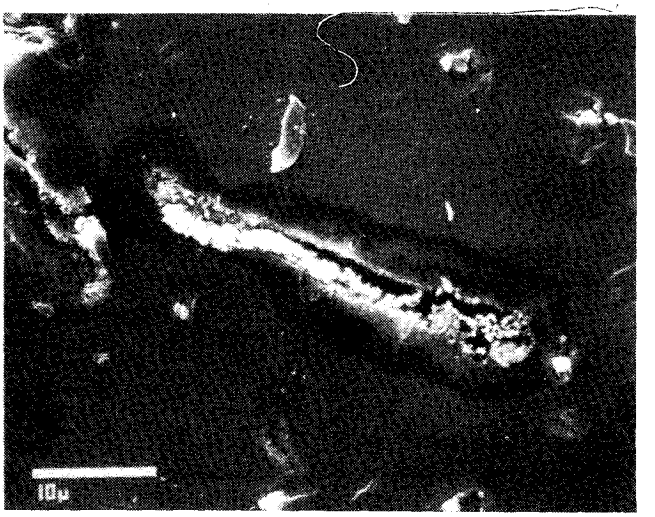

Fig. 7. Micrograph taken at 2000× of a feature on the same sample as depicted in Fig. 6. Oxidative undercutting can be seen clearly as the darkened "rim" surrounding the elongated defect.

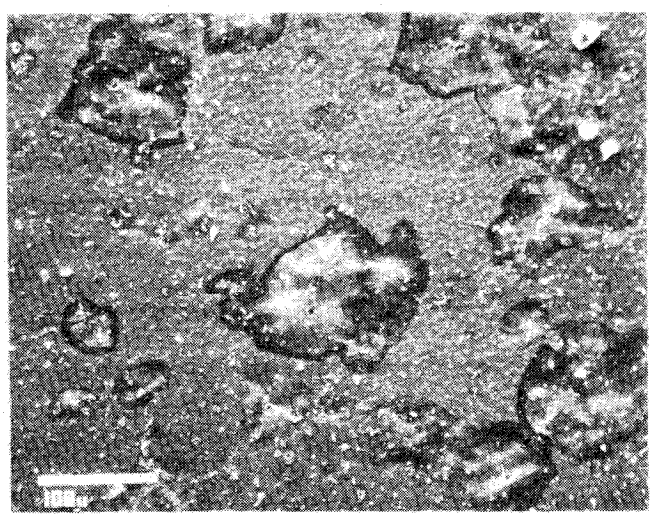

Fig. 8. Micrograph taken at 200× showing a particle eroded surface after 240 h of exposure to the oxygen plasma. The darkened areas surrounding the defect sites have grown considerably in size relative to the size of the pinhole, indicating that oxidative undercutting has occurred to a significant degree.

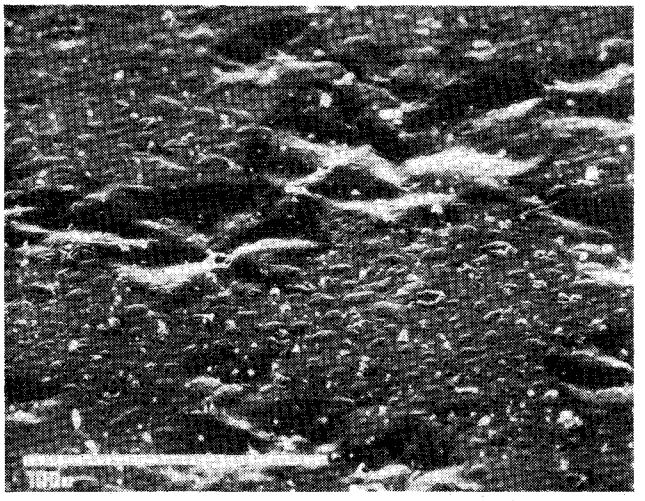

Fig. 9. Micrograph taken at 500× of the lower right portion of Fig. 8 at a sharp angle (60 deg) shows that wherever undercutting had occurred, the surface had collapsed.

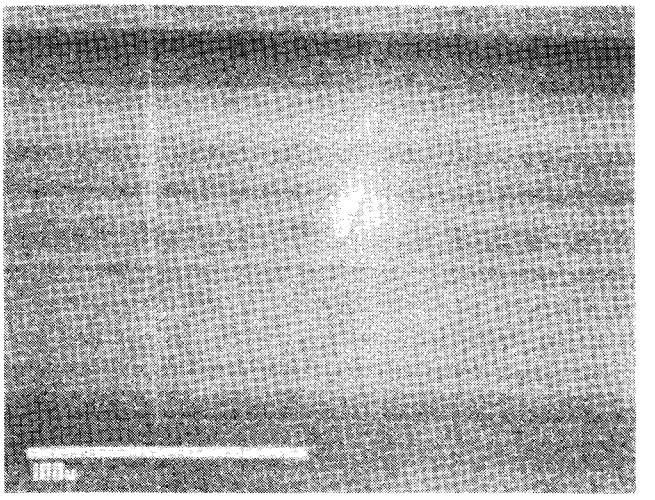

Fig. 10. Micrograph taken at 500× showing a noneroded, nonashed fused quartz substrate sample.

later, rapid falloff in reflectance. As a final observation in this series, Fig. 9 is a micrograph of the lower right portion of Fig. 8, taken at a tilt angle of 60 deg. This figure shows that wherever the undercutting occurred, the surface of the sample had collapsed. This is an indiction that oxidation of the substrate had occurred.

The series of SEM micrographs discussed above (Fig. 3–9) indicates that the reflectance data (Figs. 1 and 2) may be explained by the following mechanism: the initial, rapid drop in reflectance was caused by oxidation of those parts of the silver layer directly exposed as a result of the particle-induced damage. After some time (about 30 h in this case), this silver became completely oxidized. The reflectance then remained relatively constant for a period of time, during which oxidative undercutting had begun to occur but had not reached the point of at which the reflectance was affected. Finally, the reflectance began to fall once again as a result of undercutting of the silver layer and the substrate in undamaged areas by oxygen plasma attack through adjacent damaged areas.

Figures 10–17 show the effects of exposure of the fused quartz substrate samples to the plasma environment for different lengths of time. For comparison purposes, Fig. 10 (like Fig. 3) shows a noneroded, nonashed sample. Figure 11 is a micrograph of a sample similar to that in Fig. 10, except that it had been exposed to the particle stream. As before, a number of defect sites resulting from the particle impacts is evident. Figure 12 is a micrograph of a pitted surface after 50 h of exposure. Although no undercutting (transverse oxidation of the silver, in this case) is readily observed, oxidation of the freshly exposed silver layer is evident as the puffed material protruding from the defect sites. This is more apparent in Fig. 13, which is the same surface as shown in Fig. 12, but at a higher magnification and at a sharp tilt (60 deg).

Figure 14 is a micrograph of an eroded surface after 90 h of exposure. As before, oxidized silver protruding through the defect sites is clearly evident. Transverse oxidation of the silver after 90 h of exposure is more clearly seen in Fig. 15, which is an enlargement of Fig. 14. As in the previous samples, the oxidative damage appears as a discolored rim surrounding the defect site. In Fig. 15, the rim appears brighter in color.

Figure 16 is a micrograph showing a pitted surface after 240 h of asher exposure. As in Fig. 15, a rim lighter in color and surrounding each defect site is evident. Unlike the graphite-epoxy substrate samples, the width of the rim did not appear to increase significantly between the 90-h and 240-h samples. However, a comparison of Fig. 13 and 17—the latter is an enlargement of the same surface seen in Fig. 16 but at a 60 deg tilt—shows that the outgrowths of silver oxide had continued unabated.

Discussion

It is apparent from the preceeding results that a protective coating over substrate/silver reflector systems such as these cannot protect indefinitely against oxygen plasma-induced degradation when pinhole defects are present. The degradation observed here manifested itself in ways that were dependent on the kind of substrate material used. The samples prepared on graphite-epoxy composite, which is an oxidizable substrate, showed evidence that the substrate itself was also oxidized through the pinhole defects. This was observed in three ways. First, undercutting, once it began, occurred at a rapid rate. Second, where undercutting had occurred, the surface had collapsed (Fig. 9), indicating that the underlying support of the coating was disappearing. Third, no silver oxide was observed protruding through the defect sites. The lack of protrusion of the silver oxide is most likely because there was adequate space available beneath the protective coating for the expanding oxide in areas where the substrate itself had been oxidized.

Samples prepared on fused quartz substrates exhibited somewhat different behavior. Whereas transverse oxidation of the silver did occur, it did so at a slower rate. Also, silver oxide could be seen protruding through defect sites, indicating that there was insufficient space beneath the protective coating for the expanding oxide. This was to be expected if the substrate was not oxidizable, as was the case here.

There are several qualifying circumstances with regard to laboratory simulation of the micrometeoroid/atomic oxygen environment that must be kept in mind when interpreting these data. First, the flux of atomic oxygen in the laboratory asher is about three orders of magnitude higher than at proposed Space Station altitudes (10^{15} vs 10^{12} cm^{-2} s^{-1}).[9] On the other hand, the translational energy of the atomic oxygen in the plasma asher is only about 0.2 eV, whereas the translational energy of atomic oxygen in LEO is 4–5 eV. The consequence of these flux and energy differences is that the oxidation rate in the asher is very roughly two orders of magnitude higher than at a 465-km Space Station orbit. Second, the actual LEO micrometeoroid environment is very different from that used here.[8,10,11] The alumina particles were not accelerated to hypervelocities and, therefore, the damage sites observed may be different from what would be observed after actual micrometeoroid impacts, where it has been shown that the impacting particles line the inside of the resulting hemispherical crater.[10]

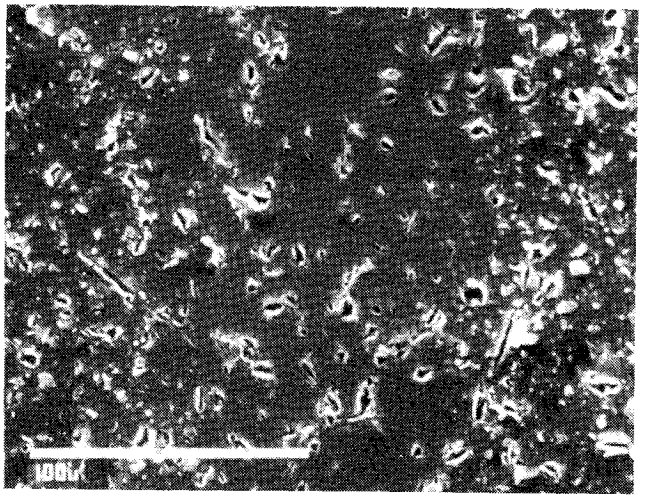

Fig. 11. Micrograph taken at 500× showing the surface of a fused quartz substrate sample after exposure to the particle stream but before exposure to the oxygen plasma.

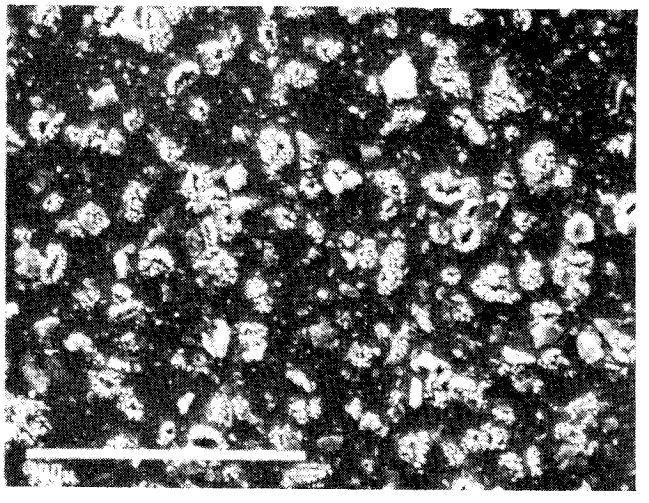

Fig. 12. Micrograph taken at 500× showing the surface of a sample identical to that of Fig. 11 but after 50 h of exposure to the oxygen plasma. Although no transverse oxidation can be seen, oxidation of the silver layer is evident as the puffy material protruding from the defect sites.

Fig. 13. Micrograph of the same sample as that of Fig. 12 but at 2000× and at 60 deg tilt angle. The oxidized silver, which takes the form of a puffy material protruding through the defect sites, is clearly evident.

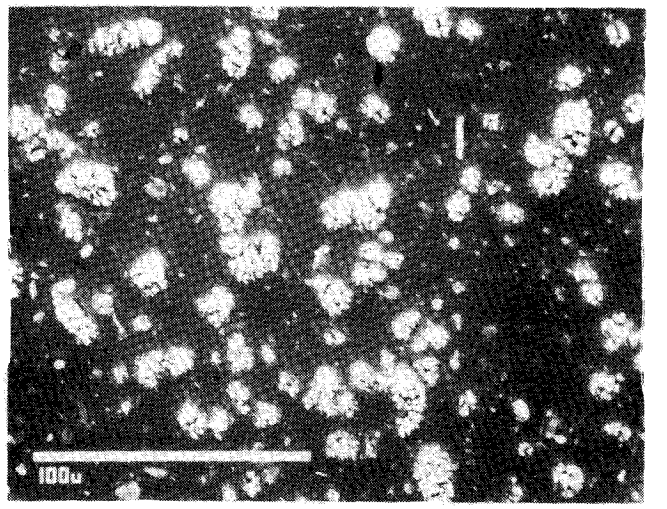

Fig. 14. Micrograph taken at 500× showing the surface of a fused quartz substrate sample after particle erosion and 90 h of exposure to the oxygen plasma. Oxidized silver is seen protruding through the defect site. Transverse oxidation is visible as a brighter rim surrounding the defect site.

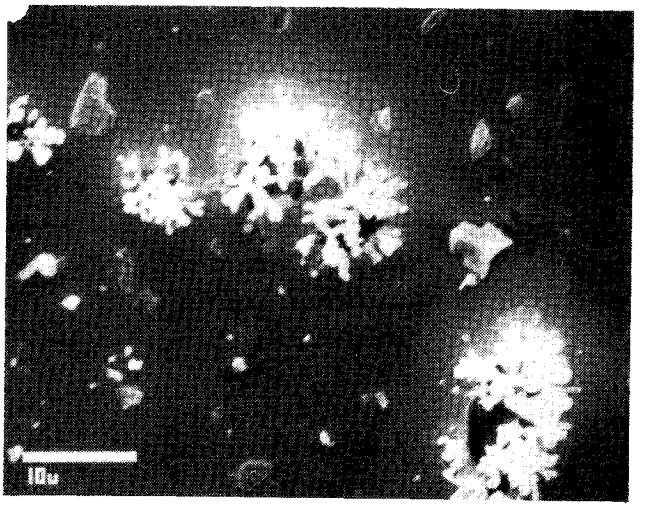

Fig. 15. Micrograph of the same sample as that of Fig. 14 but at 2000×. Transverse oxidation is clearly evident as a brighter rim surrounding the defect site.

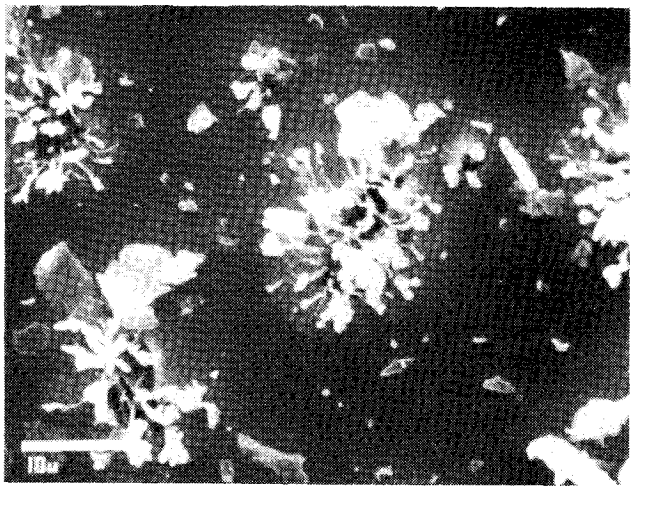

Fig. 16. Micrograph taken at 2000× showing the surface of a fused quartz substrate sample after particle erosion and 240 h of oxygen plasma exposure. Transverse oxidation is evident; however, its extent did not increase significantly over that of the 90-h sample (Figs. 14 and 15).

Fig. 17. Micrograph of the same sample as that of Fig. 16 at the same magnification and a 60 deg tilt. Outgrowth of oxidized silver had been continuing as of 240 h.

In spite of these differences, useful information can be inferred about the construction of a reflective system for use in LEO. The presence of an oxidation "barrier" (the quartz substrate) beneath the silver layer prevented the rapid spread of oxidative damage. This suggests that to prevent or retard oxidative damage to the graphite-epoxy substrate (and, subsequently, the reflective layer surrounding a defect site), a layer of oxidation-resistant material should be placed between the substrate and the silver layer. Such a coating structure would be, in effect, identical to the quartz substrate systems studied here, and it should function similarly, as long as the impacting particle does not pierce this oxidation barrier layer. Investigation of a layer structure such as this has been initiated at this laboratory.

It is also important to recognize other sources of pinhole defects besides those occurring once the mirror is in orbit. It is at least as likely that such defects could occur as a result of the manufacture, transport, and/or deployment of the mirror. Given the several possible sources of defect damage to reflector surface protective coatings, and given the aforementioned uncertainties in relating the actual LEO atomic oxygen/micrometeoroid environment to laboratory simulations, actual on-orbit tests of mirror samples will be necessary to determine both actual reflectance loss rates and the relationship of these laboratory simulations to actual LEO conditions.

Acknowledgment

The author would like to acknowledge several useful discussions with Dr. Donald J. McClure of 3M Corporation, who suggested the idea of an oxidation barrier layer.

References

[1] *U.S. Standard Atmosphere, 1976,* U.S. Government Printing Office, Washington, DC, 1976, p. 30.

[2] Banks, B.A., Mirtich, M.J., Rutledge, S.K., Swec, D.M., and Nahra, H.K., "Protection of Solar Array Blanket from Attack by Low Earth Orbital Atomic Oxygen," *Proceedings of the 18th IEEE Photovoltaic Specialists Conference,* IEEE, New York, 1985, pp. 381–386.

[3] Leger, L.L., "Oxygen Atom Reaction with Shuttle Materials at Orbital Altitudes," AIAA Paper 83-0073, 1983; see also NASA TM-58246, 1982.

[4] Whitaker, A.F., "LEO Atomic Oxygen Effects on Spacecraft Materials," AIAA Paper 83-2632, 1983; see also NASA TM-86463, 1984.

[5] Gulino, D.A., "Ion Beam Sputter Deposited Zinc Telluride Films," *Journal of Vacuum Science and Technology A*, Vol. 4, May–June 1986, pp. 509–513.

[6] Rutledge, S.K., Banks, B.A., DiFilippo, F., Brady, J.A., Dever, T.M., and Hotes, D., "An Evaluation of Candidate Oxidation Resistant Materials for Space Applications in LEO," Paper presented at the NASA Workshop on Atomic Oxygen Effects, Pasadena, CA, Nov. 1986; NASA TM (to be published).

[7] Raushenback, H.S., *Solar Cell Array Design Handbook,* Van Nostrand-Reinhold, New York, 1980, p. 411.

[8] Mirtich, M.J. and Mark, H., "The Effect of Hypervelocity Projectile Material on the Ultimate Reflectance of Bombarded Polished Metals," NASA TM X-52981, 1971.

[9] Ferguson, D.C., "The Energy Dependence and Surface Morphology of Kapton Degradation Under Atomic Oxygen Bombardment," *Proceedings of the 13th Space Simulation Conference,* NASA CP-2340, 1984, pp. 205–221.

[10] Bowman, R.L., Mirtich, M.J., and Weigand, A.J., "Changes in Optical Properties of Various Transmitting Materials Due to Simulated Micrometeoroid Exposure," NASA TM X-52687, 1969.

[11] Mirtich, M.J. and Bowman, R.L., "Effect of Simulated Micrometeoroid Exposure on Performance of N/P Silicon Solar Cells," *AIAA Journal,* Vol. 5, July 1967, pp. 1364–1366.